DESIGN AND DEVELOPMENT OF AN OPEN-SOURCE HARDWARE DIGITAL OXYGEN FLOW CONTROLLER FOR RESPIRATORY THERAPY

NOOR, A. M.

Faculty of Electronic Engineering & Technology, Universiti Malaysia Perlis, Perlis, Malaysia.
e-mail: anasnoor[at]unimap.edu.my

(Received 28th November 2025; revised 20th February 2026; accepted 08th March 2026)

Abstract. Conventional oxygen flow controllers rely on manual knob adjustment and separate devices for neonatal and adult patients, increasing equipment costs, complicating clinical workflows, and adding maintenance burdens. To address these challenges, we developed a unified, low-cost, open-source digital oxygen flow controller capable of regulating oxygen delivery from 0.1 to 15 LPM. The system is constructed using readily available components, including a stepper motor, a flow sensor, and a microcontroller, and employs a Proportional–Integral–Derivative (PID) feedback control algorithm to achieve precise real-time flow regulation. The open-source hardware and firmware architecture enhances transparency and reproducibility while providing a flexible platform for future research involving closed-loop feedback systems, in which oxygen flow rates can be automatically adjusted in response to patient-specific physiological signals. Experimental validation demonstrated robust performance across the full therapeutic range. For flow rates between 1 and 15 LPM, delivered flows closely matched setpoints with low variability, and Bland–Altman analysis indicated a consistent bias of 0.02 LPM with narrow limits of agreement. In the neonatal range (0.1–1.0 LPM), measurement deviations were generally below 8%. These findings confirm that a simple, open-source, component-based digital design can deliver accurate and predictable oxygen flow control for both neonatal and adult respiratory therapy, offering a cost-effective and extensible foundation for advanced feedback-controlled oxygen delivery and future integration with patient monitoring and adaptive respiratory support systems.
Keywords: *open source hardware, flow controller, respiratory therapy, oxygen therapy, medical device*

Introduction

Respiratory therapy is a critical multidisciplinary field involving physicians, nurses, and respiratory therapists who collectively manage the assessment, treatment, and pre-vention of respiratory disorders. These conditions range from chronic diseases such as asthma and Chronic Obstructive Pulmonary Disease (COPD) to acute emergencies requir-ing immediate respiratory support (DiBlasi and Gallagher, 2016). Central to these interventions is oxygen therapy, whose efficacy depends on precise titration of flow rates tailored to patient age, physiolo-gy, and clinical status. In adults, oxygen is typically administered via nasal cannulae at 1–6 L/min and up to 15 L/min with simple or reservoir masks (Weekley et al., 2025; Ernstmeyer and Christman, 2023). By contrast, neonates and pediatric patients require substantially lower and more tightly regulated flows. The World Health Organiza-tion recommends 0.5–1 L/min for neonates, 1–2 L/min for infants, and 2–4 L/min for older children, usually delivered through nasal prongs or small face masks (WHO, 2016). Previous studies using neonatal airway models corroborate that flows between 0.5–2 L/min are both safe and effective when delivered via neonatal cannulae (Sabz et al., 2022). These differences underscore the demand for oxygen delivery systems that can accommodate a broad spectrum of flow re-quirements with high fidelity.

Accurate oxygen titration is especially critical in patients with COPD, acute respiratory distress syndrome (ARDS), severe pneumonia, and neonatal respiratory

distress, where both inadequate and excessive oxygen delivery can worsen outcomes. Even modest deviations from the prescribed flow or saturation targets may trigger hypoxia, oxidative tissue injury, or hyperoxia, risks that are particularly dangerous in neonates and critically ill patients, including those with COVID-19–associated ARDS (Dushianthan et al., 2023; Lellouche et al., 2013). Clinical workflows are further complicated by the lack of a single oxygen delivery platform that can safely serve both neonatal and adult patients, necessitating the use of multiple devices optimized for different flow ranges and clinical contexts. In practice, clinicians must switch between devices based on differing operating principles, such as rotary or pressure regulators, Thorpe tube flowmeters, and other analog flow-control systems, each with its own calibration and handling requirements. These device transitions expand training demands, can slow time-critical interventions, and contribute to flow-setting inaccuracies and dosing errors, particularly at low or very high flows (Duprez et al., 2021; 2014). Conventional regulators, including float-type flow controllers, provide acceptable precision under certain conditions but frequently lose accuracy at the low flow ranges re-quired in neonatal care. A multicenter field study involving flow controller devices re-ported considerable inter-device variability at low flows, necessitating frequent recalibra-tion and discouraging cross-device interchangeability. Similarly, an in vitro evaluation of Thorpe tube flow controllers demonstrated high precision but poor accuracy at flows of 1–3 L/min, revealing inconsistency even within the same model type. Routine recali-bration and maintenance further add to operational burdens, particularly in high-demand clinical environments where interruptions can compromise patient care and increase costs (Davidson et al., 2012).

An oxygen delivery solution must combine wide flow-range capability with high accuracy, minimal manual adjustment, and reduced operational complexity. For pediatric and neonatal patients in particular, digital oxygen flow controllers that integrate advanced sensing with closed-loop algorithms are not optional but essential for safe therapy (Sandal et al., 2022). Feedback-enabled oxygen therapy systems are critical because they continuously adapt to fluctuating patient needs such as in acute hypoxemic respiratory failure (AHRF) where studies have shown that automated control significantly improves stability and outcomes compared to manual adjustment (Roca et al., 2022). Flowmeter inaccuracy affects both adult and neonatal populations by preventing achievement of narrow, evidence-based oxygen saturation targets the foundation of modern oxygen therapy. In adults with COPD, flowmeter error contributing to SpO_2 drift above 92% associates with 98–197% increased in-hospital mortality. In neonates, the same device inaccuracy produces its worst performance (48–185% error) at the critical 2 L/min setting, undermining oxygen saturation targets and predisposing to bronchopulmonary dysplasia and retinopathy of prematurity. With 31–35% of medical-grade flowmeters operating outside international standards, addressing device accuracy is essential to realizing the benefits of evidence-based oxygen therapy across all ages (Echevarria et al., 2021). This work presents the development of a low-cost, open-source digital oxygen flow controller designed to operate across a wide flow range of 0.1–15 L/min. The device is intended to provide accurate oxygen regulation for both neonatal and adult applications within a single platform, reducing the need for multiple regulators. A Proportional–Integral–Derivative (PID) control algorithm is implemented to stabilize flow in real time, thereby minimizing reliance on manual adjustment and reducing potential variability. By combining broad flow capability with automated feedback control, the system aims to improve both accuracy and usability. In

addition, the open-source, component-based architecture supports transparency, reproducibility, and future extensibility, offering potential for deployment in both advanced hospitals and resource-limited healthcare settings.

Materials and Methods

Proposed system and controller

This section outlines the components, system architecture, and experimental procedures for the design and evaluation of the proposed digital oxygen flow controller. The hardware configuration consists of a microcontroller, proportional control valve, flow sensor, pressure sensor, display unit, and power supply. Each component was selected according to technical specifications suitable for continuous oxygen delivery, and their functional roles within the integrated system are described to show how hardware and control elements interact. The methods include system design, control algorithm ross a therapeutic range of 0.1 L/min for neonatal use to 15 L/min for adult high-flow therapy. Performance was evaluated through controlled bench testing with measurements obtained at multiple flow settings under simulated clinical conditions. The device was assessed for stability, repeatability, and consistency of flow delivery, and the results were compared against a standardized reference flowmeter. The ESP32 microcontroller was selected as the central control unit for its high pro-cessing capability, integrated wireless communication, and extensive I/O support, making it well-suited for real-time oxygen flow regulation. It acquires the user-defined target flow rate via a membrane keypad and displays system status on a TFT module, while simulta-neously driving a stepper motor through a dedicated motor driver to actuate a mechanical control valve with high positional precision. Real-time flow measurements from the SFM3300-D digital mass flow sensor are acquired via the I²C protocol and processed by a Proportional–Integral–Derivative (PID) control algorithm to minimize the error between target and measured flow rates. This closed-loop control maintains flow accuracy within ±0.05 L/min across the full operational range, ensuring stable, responsive, and reliable oxygen delivery.

Valve control mechanism

The NEMA 17HS4401 stepper motor was selected for valve actuation due to its bal-ance of resolution, torque, and integration suitability. It has a step angle of 1.8° (200 steps per revolution), enabling fine control of the valve opening and stable oxygen flow delivery. The motor provides a holding torque of 45 N·cm, sufficient to resist backpressure, while its rated current of 1.7 A per phase and low inductance windings support consistent torque output with minimal heat generation. Its low cost, wide availability, and compatibility with common drivers further strengthen its suitability for scalable oxygen flow controller development. The TB6600 stepper motor driver serves as the interface between the ESP32 microcon-troller and the NEMA 17HS4401 stepper motor, converting low-voltage logic signals into the higher voltage and current required for motor actuation. The driver supports adjusta-ble step resolution and drive current, enabling stable valve positioning for controlled oxy-gen delivery. In this implementation, it was configured for 1/16 microstepping, corre-sponding to 3200 pulses per revolution, which provides a practical balance between posi-tional resolution and responsiveness. It supports input pulse frequencies up to 200 kHz, allowing rapid

response to control signals and enabling fast adjustments in valve position when flow setpoints are changed. Its broad compatibility with standard stepper motors and flexible microstepping options further enhance integration, scalability, and ease of maintenance in medical device applications.

The SFM3300-D digital flow sensor was integrated downstream of the control valve to provide real-time measurement of oxygen flow for closed-loop regulation. It supports a wide measurement range up to 250 L/min, which comfortably covers the therapeutic re-quirement of 0.1 to 15 L/min for both neonatal and adult oxygen therapy. The sensor offers high accuracy with a typical response time below 5 ms, ensuring that flow deviations are detected and corrected promptly by the controller. Communication with the ESP32 micro-controller is established through a digital I²C interface, allowing direct data transfer without external signal conditioning. While flow sensing is inherently influenced by gas temperature and humidity, the sensor incorporates built-in temperature compensation that preserves measurement stability across its operating range of –20 °C to +70 °C. These fea-tures enable reliable and repeatable feedback for oxygen flow control applications in clin-ical settings. The Festo GR-QS-4 mechanical valve functions as the core flow control element, driven by the NEMA 17 stepper motor to regulate oxygen delivery. Its 0.4 mm internal bore was selected to provide fine resolution at low flow rates, a critical requirement for neonatal oxygen therapy. The valve maintains a linear and repeatable relationship between dis-placement and flow rate, allowing predictable modulation within the closed-loop control system. Bench evaluation confirmed that it can sustain flow rates up to 110 L/min while maintaining stable characteristics. In addition, the valve is rated for operating pressures up to 10 bar, which far exceeds the typical downstream oxygen therapy pressure range of 0.3–0.5 bar. This high-pressure tolerance ensures structural safety, prevents leakage, and guarantees durability during extended clinical use. Its compact and mechanically robust design further supports long-term reliability under repeated actuation, making it a suitable choice for integration in this system.

User interface

A 2.8-inch TFT LCD module driven by the ST7789 controller was selected to provide real-time visualization of key system parameters. The display outputs the user-defined set flow value, the measured instantaneous flow from the sensor, and system action messages such as Flow ON or Flow Stop. With a resolution of 240 × 320 pixels and support for 65K colors, the module offers high readability and contrast, which is important for immediate interpretation by healthcare personnel in varied ambient lighting conditions. The SPI-based communication interface ensures rapid refresh rates while maintaining low computational overhead for the ESP32 microcontroller. User input is achieved through a 4 × 4 membrane keypad, which supports direct nu-meric entry of target flow values. This interface eliminates reliance on incremental scroll-ing or toggling, thereby reducing adjustment time and minimizing input errors. Its sealed flat-surface construction is resistant to fluid ingress and facilitates disinfection, making it suitable for repeated clinical use. The combination of the TFT display and keypad pro-vides a clear, responsive, and hygienic interface optimized for oxygen flow control appli-cations. A 12 V, 3000 mAh lithium-ion battery serves as the primary power source, supplying direct power to the stepper motor and driver, ensuring stable and reliable operation across all components. Voltage regulation is provided by an MB102 module, which delivers 5 V for the flow sensor, 3.3 V for the ESP32 microcontroller,

and maintains 12 V for the motor subsystem. This configuration supports stable multi-rail distribution, minimizes voltage drop during peak motor loads, and isolates the control and sensing circuits from mo-tor-induced electrical noise.

Flow control algorithm and device casing design

The control software was implemented on the ESP32 microcontroller using the Ar-duino development environment, structured into modular routines for sensor acquisition, user interaction, control computation, and actuator output. Flow rate data from the SFM3300-D sensor are sampled at a fixed acquisition rate and filtered to suppress high-frequency noise before entering the control loop. User input from the membrane key-pad defines the target flow setpoint, which is continuously compared against the meas-ured flow. A digital proportional–integral–derivative (PID) algorithm computes the control signal, dynamically adjusting the stepper motor position to modulate valve opening. The control output is transmitted to the TB6600 driver through pulse and direction signals, enabling micro-stepped actuation with millisecond-scale response. The algorithm priori-tizes stability at low flow rates critical for neonatal therapy while maintaining respon-siveness across the full therapeutic range up to 15 L/min. Real-time system feedback, in-cluding the commanded flow, actual flow, and operational status messages, is rendered on the TFT display to support direct monitoring and verification.

The mechanical design of the proposed device was developed to ensure clinical safe-ty, structural durability, portability, and ergonomic usability in healthcare environments. The device casing was modeled using SolidWorks CAD software to enable precise com-ponent integration, iterative design evaluation, and optimization of internal layout. The finalized design was fabricated using 3D printing with ABS thermoplastic filament, a ma-terial selected for its high impact resistance, mechanical strength, and suitability for fre-quent handling in clinical workflows. The casing incorporates a compact rectangular en-closure (16 cm × 15 cm × 10 cm) with softly rounded edges, minimizing the risk of acci-dental injury during handling. A built-in side handle improves portability, allowing healthcare staff to easily transport the device between patients or wards. The internal ar-chitecture was arranged with modularity in mind, providing direct access to critical com-ponents including the flow sensor, FESTO valve, and Li-ion battery facilitating rapid maintenance or replacement. Safety considerations were prioritized in the enclosure design. High-voltage compo-nents, such as the 12 V Li-ion battery and TB6600 motor driver, were physically isolated within protective compartments and connected using insulated wiring to reduce electrical hazards. Ventilation slots were integrated near the motor driver to enable passive heat dissipation, ensuring reliable thermal management during continuous operation. Exter-nally, the user interface is ergonomically arranged, the ST7789 TFT display is mounted on the upper front panel to provide real-time feedback, while the 4×4 membrane keypad is positioned directly below for intuitive user input. A dedicated RCA charging port and power switch are positioned on the left panel for convenient access, while the stable base design accommodates the internal battery, lowering the center of gravity for improved sta-bility during use. The final prototype enclosure was printed in multiple sections and as-sembled to form a robust yet lightweight housing.

System architecture and components with circuit diagram

Built on a closed-loop control architecture, the device integrates a pneumatic pressure regulator, a stepper-motor–driven proportional valve, a digital mass flow sensor, a micro-controller unit (MCU), and a user interface module. Flow regulation is performed by a me-chanical valve (GR-QS-4, Festo, Germany) coupled to a NEMA 17 stepper motor (17HS4401, StepperOnline, China), selected for its resolution and torque characteristics required for fine aperture control under continuous backpressure. The motor is driven by the ESP32-WROOM-32 MCU (Espressif Systems, China) through a dedicated stepper driver, with the valve mechanically configured to remain closed when unpowered to pre-vent unintended oxygen delivery. Flow sensing is achieved using a digital mass flow sensor (SFM3300-D, Sensirion AG, Switzerland), which communicates with the MCU via the I²C protocol, providing high-resolution real-time flow feedback. A 4×4 membrane keypad enables direct numeric entry of setpoints, while a 2.8-inch TFT LCD (ST7789 driver, Waveshare, China) displays both the target and measured flow values alongside system status messages. Closed-loop regulation is executed by a Proportional–Integral–Derivative (PID) algo-rithm embedded on the MCU. Continuous comparison of setpoint and sensor feedback drives incremental motor adjustments, ensuring stable valve positioning and minimizing flow fluctuations. Bench evaluation demonstrated regulation across the full operational range (0.1–15 L/min), maintaining flow within ±0.05 L/min. This architecture provides fast response, reliable operation, and scalability for applications spanning neonatal to adult oxygen therapy. *Figure 1* presents the architecture of the proposed digital oxygen flow controller.

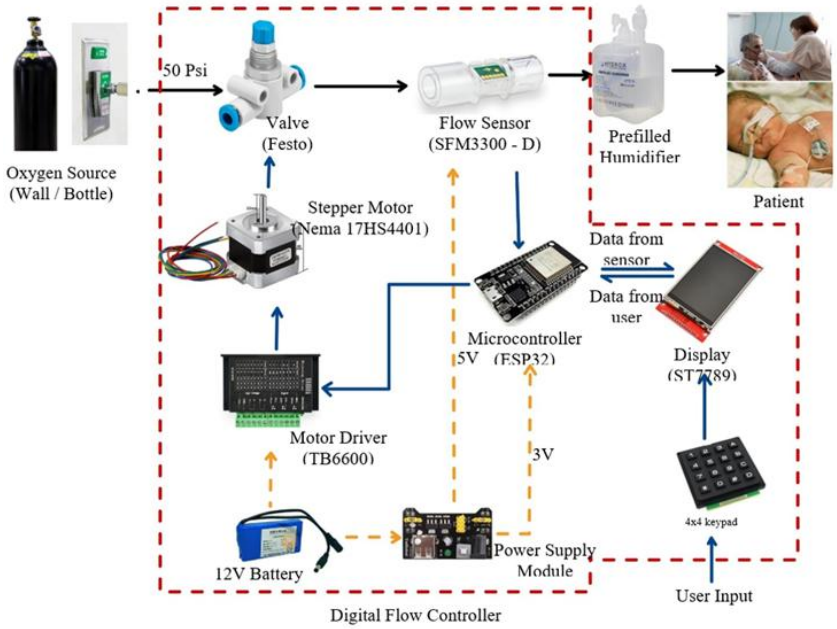

Figure 1. *Architecture of the proposed digital oxygen flow controller.*

The electrical subsystem is centered on the ESP32-WROOM-32 microcontroller, which synchronizes flow sensor feedback, user interface inputs, and stepper motor actuation. Power is supplied by a 12 V Li-ion battery, with regulated outputs distributed to the motor driver, sensor circuitry, and logic-level control modules. Communication between periph-erals is implemented using I²C for the flow sensor, SPI for the display, and digital I/O for motor control, all referenced to a common ground to minimize signal

noise and ensure re-liable operation. The wiring topology is arranged in a modular configuration with short, shielded interconnects to reduce electromagnetic interference, facilitate debugging, and simplify future maintenance. *Figure 2* shows the schematic diagram of the device electron-ics, and *Table 1* lists the corresponding component pin connections.

Table 1. *Device component link.*

Connection Pin	MB102	ESP32	SPM3300-D	TB6600	17HS4401	ST7789	KEYPAD
ESP⇔ST7789		40		10	A+	9	
ESP⇔SPM3300 // TB6600⇔17HS4401		39	3	9	A-		
ESP⇔SPM3300 // TB6600⇔17HS4401		36	5	8	B+		
ESP⇔ST7789 // TB6600⇔17HS4401		30		7	B-	8	
ESP⇔ST7789		29				12	
ESP⇔ST7789		26				11	
ESP⇔ST7789		23				10	
ESP⇔TB6600		19		4			
ESP⇔TB6600		17		6			
ESP⇔KEYPAD		14					C1
ESP⇔KEYPAD		13					C3
ESP⇔KEYPAD		12					C2
ESP⇔KEYPAD		11					C0
ESP⇔KEYPAD		10					R3
ESP⇔KEYPAD		9					R2
ESP⇔KEYPAD		8					R1
ESP⇔KEYPAD		7					R0
VCC 3.3V	2	1				14	7
VCC 5V	3		2				
VCC 12	1			12			
GND	4	41	4	11/3/5		13	

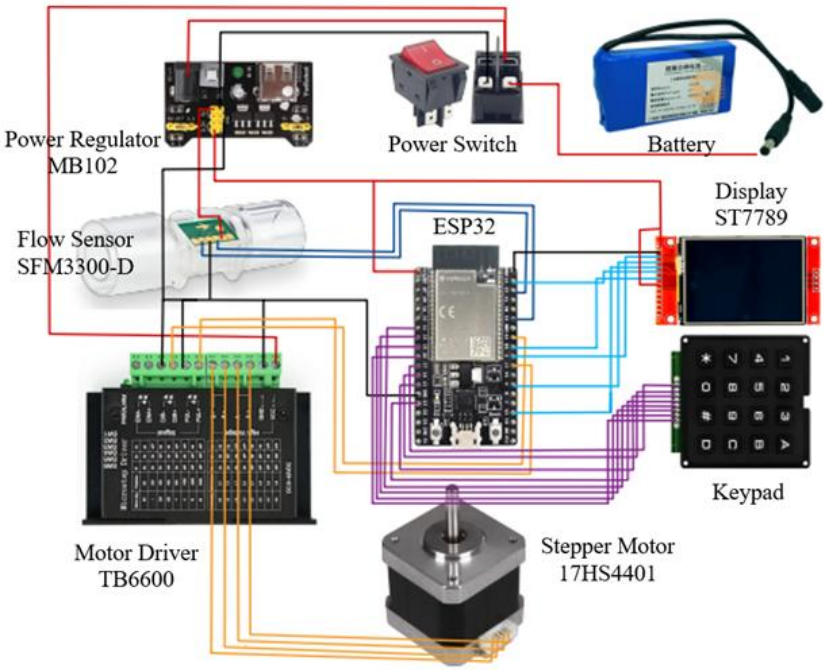

Figure 2. *Schematic circuit diagram.*

Flow control algorithm

The ESP32-WROOM-32 microcontroller implements a closed-loop flow regulation system that integrates keypad input, real-time flow sensing, and valve actuation. After

pe-ripheral initialization, the controller operates in two selectable ranges Neonatal (0.1–2.0 SLPM) and Adult (1.0–15.0 SLPM) to optimize resolution across clinical applications. Target flow values entered by the user are continuously compared against instantaneous feedback from the SFM3300-D digital mass flow sensor. A Proportional–Integral–Derivative (PID) algorithm computes the error signal and generates step and direction pulses to the TB6600 driver, which actuates the NEMA 17 stepper motor and modulates the FESTO GR-QS-4 valve aperture. *Figure 3* presents the flowchart of the control algorithm for the proposed device. The PID structure provides fast, accurate, and stable control, the proportional term delivers rapid correction to deviations, the integral term eliminates steady-state error, and the derivative term anticipates error trends to suppress overshoot and oscillation. With properly tuned gains, the system maintains delivery accuracy within ±0.05 SLPM over the full operating range (0.1–15.0 SLPM) and responds effectively to flow disturbances, back-pressure variations, or sudden load changes. The PID control algorithm is shows in *Figure 4*.

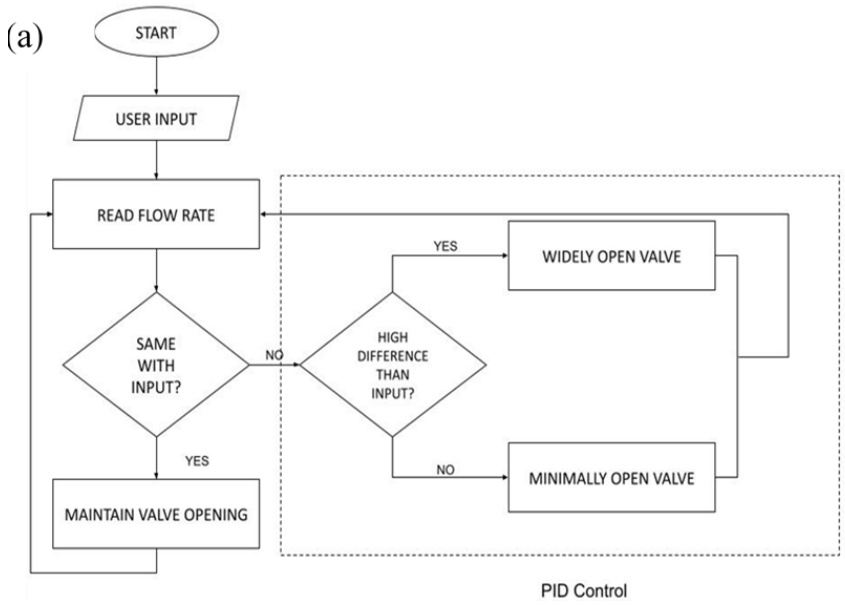

Figure 3. *Flow control algorithm flowchart.*

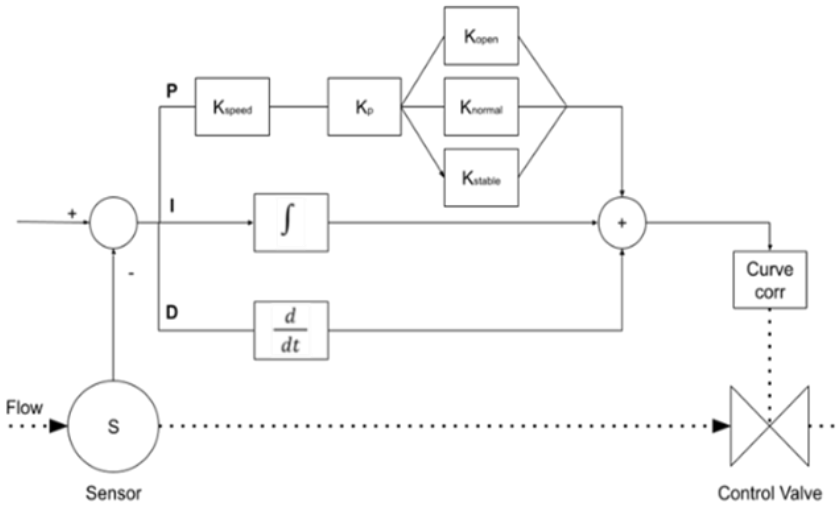

Figure 4. *Flow control algorithm of PID functional structure.*

The closed-loop oxygen flow regulation system is governed by a Proportional–Integral–Derivative (PID) control strategy. In continuous time, the control law is expressed as Eq. (1)

$$u(t) = K_p \cdot e(t) + k_i \int_0^t e(\tau)d\tau + K_d \cdot \frac{de(t)}{dt} \quad \text{Eq. (1)}$$

Where; u(t)=Control signal sent to the stepper motor driver (pulse rate or direction); e(t)=SP(t)-PV(t)=Instantaneous error between desired and actual flowrate; K_p=Proportional gain-controls immediate error correction; K_i=Integral gain-eliminates steady-state error by considering past errors; K_d=Derivative gain-predicts future error and adds damping to the system. Since the ESP32 microcontroller operates in discrete time, the PID algorithm for the Digital Oxygen Flow Controller is implemented in a sampled form, as expressed in Eq. (2):

$$u(n) = K_p \cdot e[n] + k_i \cdot \sum_{k=0}^{n} e[k] \cdot \Delta t + K_d \cdot \frac{e[n] - e[n-1]}{\Delta t} \quad \text{Eq. (2)}$$

This output u[n] is translated into stepper motor movement to increase or decrease the valve opening, thereby adjusting the oxygen flow to match the setpoint. The values of K_p, K_i, and K_d were experimentally tuned to achieve the desired performance. These enable precise control in neonatal ranges (0.1–2.0 SLPM), where small fluctuations are clinically significant, while supporting higher responsiveness in adult therapy ranges (3.0–15.0 SLPM). The closed-loop system continuously monitors real-time flow, computes error, and updates control signals to compensate for drift, disturbances, or backpressure variations, thereby ensuring stable, accurate, and safe oxygen delivery.

Results and Discussion

Performance evaluation

The performance of the device was systematically evaluated to establish its accuracy, reliability, and consistency across a clinically relevant flowrate spectrum, spanning neo-natal oxygen therapy (0.1–2.0 LPM) and adult oxygen therapy (3–15 LPM). The evaluation aimed to confirm that the developed system performs with comparable fidelity to a con-ventional reference flowmeter (SMC, PFM725, Japan) under controlled laboratory condi-tions. To achieve a comprehensive assessment, three complementary methods were applied; mean and standard deviation analysis, percentage difference analysis, and Bland–Altman analysis, providing a rigorous validation of clinical suitability and robustness. For each tested flowrate, both the proposed device and the reference device were as-sessed over five repeated trials. The mean flowrate was computed to evaluate the average performance of each device, while the standard deviation (SD), calculated using Eq. (3), quantified the variability from the mean. A low SD value reflects high repeatability and measurement stability. To account for differences across magnitudes of flow, the coefficient of variation (CV) was determined

according to Eq. (4), providing a normalized measure of dispersion and enabling consistent comparison across both neonatal and adult flow ranges.

$$SD = \sqrt{\frac{1}{n-1}\sum_{i=1}^{n}(x_i - \bar{x})^2} \quad \text{Eq. (3)}$$

$$CV\% = \left(\frac{SD}{\bar{x}}\right) \times 100 \quad \text{Eq. (4)}$$

The alignment of the device with the SMC was further assessed through percentage difference analysis, which directly quantified the relative deviation between the mean readings of both devices at each flowrate shown in Eq. (5). This method provides a straightforward indicator of accuracy, ensuring that the developed system operates within clinically acceptable tolerance limits for oxygen therapy applications. Finally, Bland–Altman analysis was conducted to evaluate the agreement and systematic bias between the two devices. This technique compared the mean of each paired measurement against their difference, calculated using Eq. (6) and Eq. (7), respectively. By identifying both the bias and the limits of agreement, this analysis determined whether the prototype can be considered interchangeable with the clinical reference standard, thereby confirming its suitability for precise and safe oxygen delivery in neonatal and adult therapy settings. The mean difference, also known as the bias, was then calculated using Eq. (8). To determine the range within which most differences are expected to lie, the limits of agreement were calculated using Eq. (9). Practically, if the majority of data points lie within the calculated limits of agreement, the proposed device is regarded as consistent with the reference system.

$$\%\ Difference = \left(\frac{|Device\ Mean - Ref.Mean|}{Ref.Mean}\right) \times 100 \quad \text{Eq. (5)}$$

$$Mean\ Pair = \frac{Device + Ref.Device}{2} \quad \text{Eq. (6)}$$

$$Difference = Device - Ref.Device \quad \text{Eq. (7)}$$

$$Bias\ (Mean\ Difference), \overline{Sd} = \frac{\sum(Device - Ref.\ Device)}{n} \quad \text{Eq. (8)}$$

$$Limit\ agreement = \bar{d} \pm 1.96 \cdot SD \quad \text{Eq. (9)}$$

Device casing

The device casing was fabricated using a 3D printer with ABS thermoplastic material, chosen for its high impact resistance, durability, and suitability for medical environments where frequent handling is required. The enclosure was designed to provide both me-chanical protection and ergonomic usability, with smooth rounded

edges to minimize the risk of accidental injury during clinical operation. From an electrical safety perspective, the casing also serves as a protective barrier, isolating high-voltage components such as the battery and motor driver from external contact. Since the device is powered by a rechargeable lithium-ion battery, safety considerations follow the general guidelines of IEC 60601 (Medical Electrical Equipment-General Safety Requirements) and IEC 62353 (Medical Electrical Equipment-Recurrent Test and Test after Repair). These standards address essential aspects such as leakage current, in-sulation, and protective earth integrity to ensure safe use in clinical environments. At pre-sent, full compliance testing according to IEC 60601 and IEC 62353 has not yet been con-ducted, but the design has been developed with these requirements in mind to facilitate future certification and safe integration into healthcare practice. *Figure 5* shows the printed casing (design file available in Supplementary Materials).

Figure 5. *Printed device casing; component assembly in the casing and TFT and keypad user interface.*

The components are arranged neatly inside the 3D-printed casing, as shown in *Figure 6*. The display and keypad are mounted on the front panel for easy access, while the flow sensor and valve are placed in the center to keep the airflow direct. The motor driver and microcontroller are fixed on the side with space for cooling, and the battery is placed at the bottom to keep the device stable. High-voltage parts such as the battery and driver are kept separate and connected with insulated wires for safety. This layout makes the de-vice safe, stable, and easy to maintenance. The flowrate setpoint of the system is configured using a 4×4 keypad as shows in *Figure 7*. The keypad includes numerical keys (0–9) and four functional keys (A–D, *, #). In this implementation, numerical keys are used for direct input of flow values, while addi-tional keys serve as command inputs. The complete step-by-step procedure for setting flow values including examples of integer and decimal input sequences, confirmation steps, and display output is provided in the Supplementary Material.

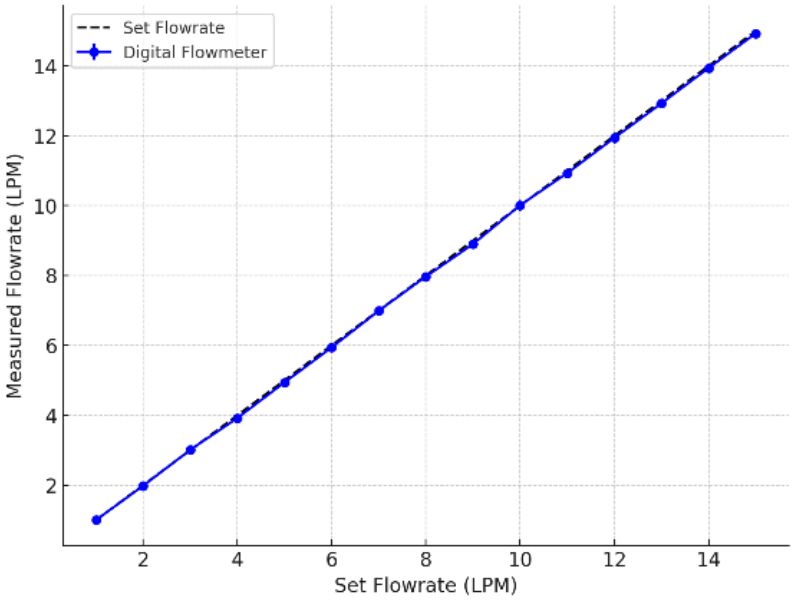

Figure 6. *Measurement of flowrate in range of 1-15 LPM.*

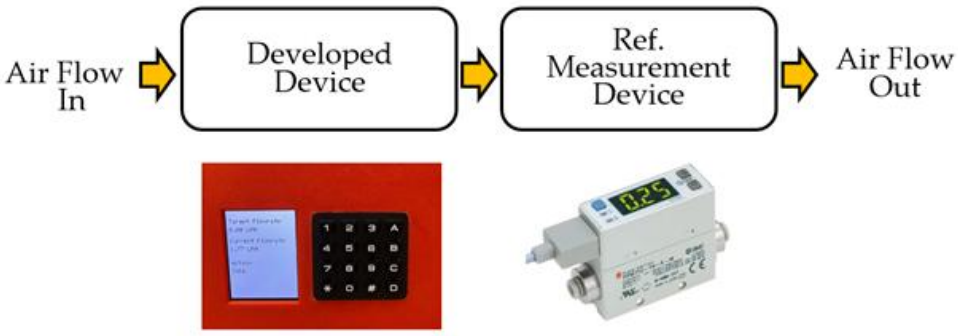

Figure 7. *Comparison of flow control by the proposed device and flow measurements obtained from the reference device.*

Device evaluation and verification

Flowrates were generated using a compressed air source regulated by a conventional manual flowmeter (Solida, BS 0–15, Thailand). The output was directed sequentially through a reference device (SMC) and then into the developed system, as illustrated in *Figure 8*. For each setpoint, five measurements were taken at 30-second intervals, and the corresponding mean, standard deviation, and coefficient of variation were calculated.

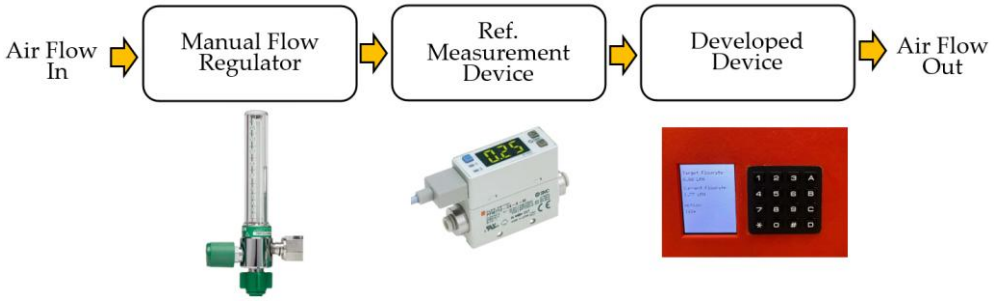

Figure 8. *Setup for comparing oxygen flow rates using ref. device.*

Mean values remained within ±0.3 LPM across the entire range, demonstrating excel-lent agreement with the imposed setpoints, as shown in *Table 2*. The device also exhibited high repeatability, reflected in low standard deviations (0.02–0.16 LPM). The coefficient of variation (CV) remained ≤3%, stabilizing at ~1% for most flowrates. This consistency in-dicates minimal variability between repeated trials and underscores the reliability of the measurement process. Overall, the results confirm that the digital flow controller achieves linear performance across the set flow range, as shown in Figure 6.

Table 2*. Flow measurement by the device.*

Set Flowrate (LPM)	Device Mean Measure (LPM)	Device SD, σ (LPM)	Device CV (%)
1.00	1.00	0.03	3.00%
2.00	1.98	0.03	2.00%
3.00	3.01	0.02	1.00%
4.00	3.92	0.05	1.00%
5.00	4.94	0.05	1.00%
6.00	5.94	0.07	1.00%
7.00	6.99	0.07	1.00%
8.00	7.97	0.10	1.00%
9.00	8.90	0.11	1.00%
10.00	10.01	0.15	1.00%
11.00	10.93	0.13	1.00%
12.00	11.94	0.16	1.00%
13.00	12.93	0.08	1.00%
14.00	13.94	0.08	1.00%
15.00	14.93	0.09	1.00%

High inlet flow conditions

Figure 7 illustrates the experimental setup in which both the developed and reference devices were tested under a constant supply of 20 LPM at 50 psi, while the control set value was sequentially adjusted from 1 to 15 LPM. *Table 3* summarizes the resulting mean flowrates obtained from both devices. The results demonstrate excellent agreement between the two systems. Across all set-points, differences were minimal, never exceeding 0.03 LPM. At the lower end of the range, the developed device measured 1.00 LPM compared with 0.99 LPM from the reference de-vice. At mid-range settings, such as 5 LPM, the readings were nearly identical (4.94 vs. 4.93 LPM). At the upper end, the devices again remained aligned, with values of 14.93 and 14.90 LPM at the 15 LPM setpoint. This consistency confirms the high fidelity of the developed system across the full operational range.

Table 3*. Flow control by the device.*

Source Flowrate (LPM)	Device Flowrate Control Set Value (LPM)	Device Mean, $\bar{x}$ (LPM)	Mean, $\bar{x}$ (Ref. Device) (LPM)
20	1	1.00	0.99
20	2	1.98	1.96
20	3	3.01	2.99
20	4	3.92	3.91
20	5	4.94	4.92
20	6	5.94	5.92
20	7	6.99	6.97
20	8	7.97	7.94
20	9	8.90	8.87
20	10	10.01	10
20	11	10.93	10.91
20	12	11.94	11.91
20	13	12.93	12.91
20	14	13.94	13.91
20	15	14.93	14.9

Low-flow regulation

Accurate quantification of low oxygen flowrates is critical in neonatal care, where therapeutic delivery typically ranges from 0.1 to 1 LPM. *Figure 9* shows the experimental setup, in which airflow was manually regulated using a neonatal flow controller (Hersil, OX1, Spain) and subsequently measured by the developed device. *Table 4* presents the mean values obtained from repeated measurements. The results confirm that the developed device can accurately measure very low flowrates below 1 LPM within acceptable error margins. As shown in *Figure 10*, airflow was regulated manually using a neonatal flow controller, while the prototype was used to capture the corresponding flowrate. No external reference was employed in this experi-ment, as the SMC sensor previously used was not suitable for ultra-low flowrates below 1 LPM. Accordingly, the results presented here represent the regulated airflow values di-rectly measured by the developed device, demonstrating its sensitivity and suitability for neonatal applications.

Table 4. *Flow measurement by the device under neonatal range.*

Set Flowrate (LPM)	Device Flowrate Mean, $\bar{x}$ (LPM)	Standard Deviation, σ (LPM)
0.10	0.10	0.00
0.15	0.10	0.01
0.20	0.19	0.02
0.25	0.23	0.00
0.30	0.29	0.01
0.35	0.33	0.00
0.40	0.36	0.02
0.50	0.43	0.00
0.60	0.58	0.01
0.70	0.70	0.00
0.80	0.78	0.01
0.90	0.88	0.02
1.00	0.97	0.00

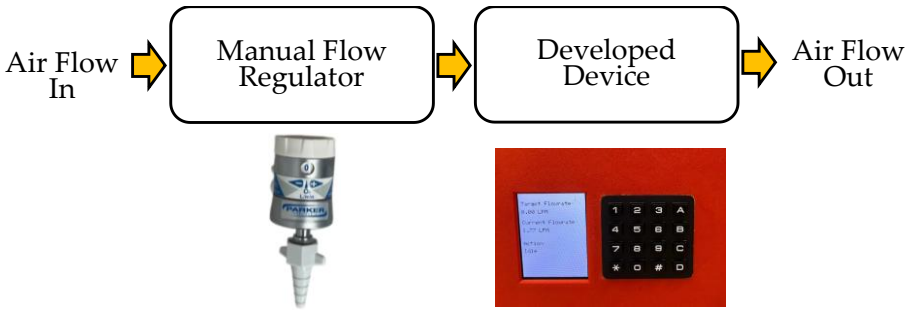

Figure 9. *Setup for comparing neonate flow rates using ref. device.*

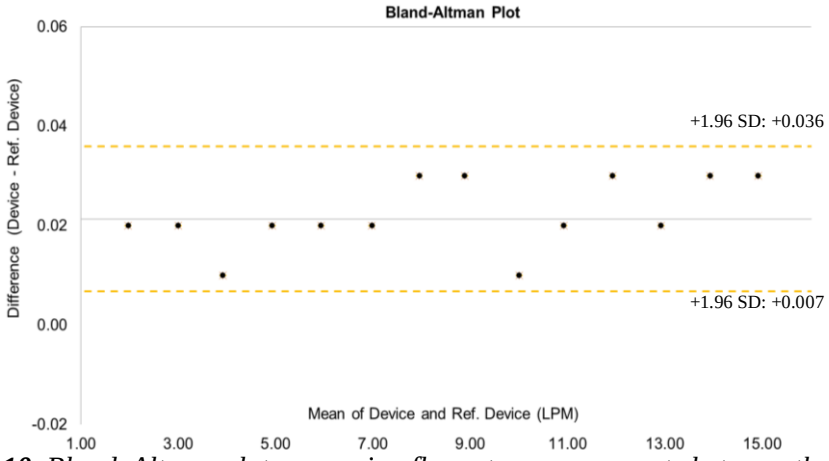

Figure 10. *Bland–Altman plot comparing flowrate measurements between the developed device and the reference device across 1–15 LPM.*

Agreement analysis using the Bland–Altman method

Bland–Altman analysis was performed to evaluate measurement agreement between the developed and reference devices across setpoints of 1–15 LPM. The mean bias was 0.021 LPM, indicating that the prototype reported slightly higher flowrates than the refer-ence. The standard deviation of the differences was 0.008 LPM, resulting in narrow 95% limits of agreement (LoA) between 0.007 and 0.036 LPM. As shown in *Figure 10*, all data points clustered closely around the bias line and fell well within the calculated LoA. No evidence of proportional bias was observed across the flow range, with differences remaining uniformly small at both lower and higher set-points. This distribution confirms that the bias is stable, predictable, and negligible for practical applications.

Conclusion

This study demonstrated the development and validation of a low-cost, open-source digital oxygen flow controller capable of delivering accurate and stable oxygen regulation across both neonatal and adult therapeutic ranges. The system exhibited reliable performance, including precise measurement and control at ultra-low flow rates below 1 LPM, confirming its suitability for sensitive neonatal applications. By adopting an open-source, component-based design using readily available hardware, the proposed controller offers meaningful potential for cost reduction, reproducibility, and wider accessibility across diverse healthcare environments. Beyond its current capabilities, the open-source architecture provides a flexible foundation for future enhancements. In particular, integration with continuous physiological monitoring modalities such as blood oxygen saturation, arterial blood gas analysis, capnography, or transcutaneous monitoring could enable closed-loop control in which oxygen delivery is automatically adjusted to patient-specific needs. Such developments would represent a significant step toward more precise, adaptive, and safer respiratory therapy systems.

Acknowledgement

This research is self-funded.

Conflict of interest

The authors confirm that there is no conflict of interest involve with any parties in this research study.

REFERENCES

[1] Davidson, J., Gazzeta, C., Torres, L.C., Jardim, J.R., Nascimento, O.A. (2012): Precision and accuracy of oxygen flow meters used at hospital settings. – Respiratory Care 57(7): 1071-1075.

[2] DiBlasi, R., Gallagher, J.T. (2016): Respiratory care of the newborn. – Assisted Ventilation of the Neonate E-Book 291p.

[3] Duprez, F., Barile, M., Bonus, T., CUVELIER, E., Ollieuz, S., Mashayekhi, S., Legrand, A. (2014): Accuracy of medical oxygen flowmeters: A multicentric field study. – Health 6: 1978-1983.

[4] Duprez, F., Dubois, A., Ollieuz, S., Cuvelier, G., Reychler, G. (2021): Thorpe tube and oxygen flow restrictor: what's flow accuracy? – Journal of Clinical Monitoring and Computing 35(2): 337-341.

[5] Dushianthan, A., Bracegirdle, L., Cusack, R., Cumpstey, A.F., Postle, A.D., Grocott, M.P. (2023): Alveolar hyperoxia and exacerbation of lung injury in critically ill SARS-CoV-2 pneumonia. – Medical Sciences 11(4): 20p.

[6] Echevarria, C., Steer, J., Wason, J., Bourke, S. (2021): Oxygen therapy and inpatient mortality in COPD exacerbation. – Emergency Medicine Journal 38(3): 170-177.

[7] Ernstmeyer, K., Christman, E. (2023): Nursing Skills [Internet]. – Open Resources for Nursing (Open RN) 962p.

[8] Lellouche, F., Lipes, J., L'Her, E. (2013): Optimal oxygen titration in patients with chronic obstructive pulmonary disease: a role for automated oxygen delivery? – Canadian Respiratory Journal 20(4): 259-261.

[9] Roca, O., Caritg, O., Santafé, M., Ramos, F.J., Pacheco, A., García-de-Acilu, M., Ferrer, R., Schultz, M.J., Ricard, J.D. (2022): Closed-loop oxygen control improves oxygen therapy in acute hypoxemic respiratory failure patients under high flow nasal oxygen: a randomized cross-over study (the HILOOP study). – Critical Care 26(1): 9p.

[10] Sabz, M., Tavernini, S., Pillay, K., Christianson, C., Noga, M., Finlay, W.H., Rouhani, H., Martin, A.R. (2022): Variability in low-flow oxygen delivery by nasal cannula evaluated in neonatal and infant airway replicas. – Respiratory Research 23(1): 10p.

[11] Sandal, O., Ceylan, G., Topal, S., Hepduman, P., Colak, M., Novotni, D., Soydan, E., Karaarslan, U., Atakul, G., Schultz, M.J., Ağın, H. (2022): Closed-loop oxygen control improves oxygenation in pediatric patients under high–flow nasal oxygen-A randomized crossover study. – Frontiers in Medicine 9: 9p.

[12] World Health Organization (WHO) (2016): Guideline: updates on paediatric emergency triage, assessment and treatment: care of critically-ill children. In Guideline: updates on paediatric emergency triage, assessment and treatment: care of critically-ill children. – WHO 74p.s

[13] Weekley, M.S., Lobo, C.M., Bland, L.E. (2025): Oxygen administration. – In StatPearls [Internet], StatPearls Publishing 2p.